

Laser-induced crystallization of β' -RE₂(MoO₄)₃ ferroelectrics (RE: Sm, Gd, Dy) in glasses and their surface morphologies

R. Nakajima^a, M. Abe^a, Y. Benino^a, T. Fujiwara^b, H.G. Kim^c, T. Komatsu^{a,*}

^a Department of Materials Science and Technology, Nagaoka University of Technology, 1603-1 Kamitomioka-cho, Nagaoka 940-2188, Japan

^b Department of Applied Physics, Graduate School of Engineering, Tohoku University, 6-6-05 Aoba, Sendai 980-8579, Japan

^c Busan Center, Korea Basic Science Institute (KBSI), Busan 609-735, South Korea

Received 9 May 2006; received in revised form 16 August 2006

Available online 17 November 2006

Abstract

The glasses with the compositions of 21.25RE₂O₃–63.75MoO₃–15B₂O₃ (RE: Sm, Gd, Dy) were prepared and the formation of β' -RE₂(MoO₄)₃ ferroelectrics was confirmed in the crystallized glasses obtained through a conventional crystallization in an electric furnace. The features of the glass structure and crystallization behavior were clarified from measurements of Raman scattering spectra. Continuous-wave Nd:YAG laser with a wavelength of 1064 nm (laser power: 0.6–0.9 W, laser scanning speed: $S = 1$ –16 $\mu\text{m/s}$) was irradiated to 10.625Sm₂O₃–10.625Gd₂O₃ (or Dy₂O₃)–63.75MoO₃–15B₂O₃ glasses, and the structural modification was induced at the glass surface. At the scanning speed of $S = 10 \mu\text{m/s}$, crystal lines consisting of β' -Gd_{2–x}Sm_x(MoO₄)₃ or β' -Dy_{2–x}Sm_x(MoO₄)₃ crystals were patterned on the glass surface. It was found that those crystal lines have the surface morphology with periodic bumps. At $S = 1 \mu\text{m/s}$, it was found that crystal lines consist of the mixture of paraelectric α -Gd_{2–x}Sm_x(MoO₄)₃ and ferroelectric β' -Gd_{2–x}Sm_x(MoO₄)₃ crystals, indicating the phase transformation from the β' phase to the α phase during laser irradiation. Homogeneous crystal lines with β' -RE₂(MoO₄)₃ ferroelectrics have not been written in this study, but further research is continuing.

© 2006 Elsevier B.V. All rights reserved.

PACS: 61.43.Fs; 78.30.–j; 81.05.Pj

Keywords: Crystallization; Crystal growth; Raman scattering; X-ray diffraction; Optical microscopy; Optical properties; Non-linear optics; Raman spectroscopy; Radiation; Rare-earths in glasses

1. Introduction

Crystallization of glass is a method for fabrication of transparent and dense condensed materials with desired shapes and also nanostructures [1]. Usually, crystallized glasses (glass ceramics) are fabricated using well-controlled heat treatment in an electric furnace and desired crystals are formed at the surface or in the interior of glass. In this kind of heat treatment methods, it is generally difficult to induce crystallization in spatially selected regions. It is of interest and of importance to develop glass/crystal hybrid

materials, in which functional (e.g., non-linear optical, ferroelectric, electronic, ferromagnetic, etc.) crystals are induced in a desired part in a given glass matrix. Such glass/crystal hybrid materials will have a high potential for practical applications in various functional devices. Laser irradiation of glass has been regarded as a process for spatially selected structural modification and crystallization in glass, and recently, various studies in laser-induced structural changes have been carried out so far, where source lasers are mainly short-wavelength excimer lasers or femtosecond pulsed lasers and structural modification are mainly refractive index changes [2–5].

The present authors' group developed a technique for laser-induced crystallization in glass, which is called samarium (rare-earth) atom heat processing [6–8]. In the samarium

* Corresponding author. Tel.: +81 258 47 9313; fax: +81 258 47 9300.
E-mail address: komatsu@chem.nagaokaut.ac.jp (T. Komatsu).

atom heat processing, continuous-wave (cw) Nd: yttrium aluminum garnet (YAG) laser with a wavelength of $\lambda = 1064$ nm is firstly irradiated to glasses containing Sm_2O_3 (or Dy_2O_3), and then, some portion of irradiated lasers is absorbed by Sm^{3+} in glass through f–f transitions (${}^6\text{F}_{9/2} \leftarrow {}^6\text{H}_{5/2}$). Since the main relaxation process from the excited state (${}^6\text{F}_{9/2}$) to the ground state (${}^6\text{H}_{5/2}$) is non-radiative (electron–phonon coupling), the laser energy absorbed by Sm^{3+} is converted to the thermal energy (lattice vibration), inducing the heating of the surrounding of Sm^{3+} . If the temperature of the laser irradiated region reaches to the crystallization temperature of a given glass, consequently crystallization is induced. Using this technique, Honma et al. [7,8] succeeded in the patterning of single-like crystal lines consisting of non-linear optical $\text{Sm}_x\text{Bi}_{1-x}\text{BO}_3$ and $\beta\text{-BaB}_2\text{O}_4$ crystals in glasses, and very recently, Ihara et al. [9] have reported the writing of two-dimensional crystal curved or bending lines consisting of $\text{Sm}_x\text{Bi}_{1-x}\text{BO}_3$ crystals showing a second harmonic generation (SHG). It is of interest to apply the samarium atom heat processing to various glass-forming systems and to induce functional crystals in glasses. Furthermore, it would be of importance to clarify the laser-induced crystallization mechanism more in detailed.

Abe et al. [10] developed $\text{Sm}_2\text{O}_3\text{–MoO}_3\text{–B}_2\text{O}_3$ glasses giving the crystallization of non-linear optical $\beta'\text{-Sm}_2(\text{MoO}_4)_3$ crystals, and, furthermore, succeeded in writing crystal lines consisting of $\beta'\text{-Sm}_2(\text{MoO}_4)_3$ using the samarium atom heat processing. Acentric rare-earth molybdates, $\beta'\text{-RE}_2(\text{MoO}_4)_3$, (RE = Pr, Nd, Sm, Eu, Gd, Tb, Dy) are well-known crystals possessing various interesting ferroelectric, ferroelastic, and non-linear optical properties [11–15]. For instance, $\beta'\text{-Gd}_2(\text{MoO}_4)_3$ crystals [11] doped with Nd^{3+} are expected as one of the promising candidates for self-frequency-doubling laser materials [16] and for making crystalline laser Raman shifters [17]. It is of interest to synthesize crystallized glasses consisting of various rare-earth molybdate $\beta'\text{-RE}_2(\text{MoO}_4)_3$ ferroelectrics. The purpose of this study is to clarify whether $\beta'\text{-RE}_2(\text{MoO}_4)_3$ ferroelectric crystals such as $\beta'\text{-Gd}_2(\text{MoO}_4)_3$ and $\beta'\text{-Dy}_2(\text{MoO}_4)_3$ are synthesized through the crystallization of $\text{RE}_2\text{O}_3\text{–MoO}_3\text{–B}_2\text{O}_3$ glasses and to write $\beta'\text{-RE}_2(\text{MoO}_4)_3$ ferroelectric crystal lines such as $\beta'\text{-Gd}_x\text{Sm}_{1-x}(\text{MoO}_4)_3$ using the samarium atom heat processing. Since $\beta'\text{-Sm}_2(\text{MoO}_4)_3$ crystal lines written by Abe et al. [10] consist of the assembly of crystals, i.e., polycrystalline $\beta'\text{-Sm}_2(\text{MoO}_4)_3$ crystal lines, we also concern on the quality (homogeneity) of $\beta'\text{-RE}_2(\text{MoO}_4)_3$ crystal lines.

2. Experimental

As reported by Abe et al. [10], the glass forming region in the $\text{Sm}_2\text{O}_3\text{–MoO}_3\text{–B}_2\text{O}_3$ system is narrow, but good glass samples can be obtained for some compositions such as 21.25 $\text{Sm}_2\text{O}_3\text{–}63.75\text{MoO}_3\text{–}15\text{B}_2\text{O}_3$ (mol%). In this study, therefore, glasses with the compositions of 21.25 $\text{RE}_2\text{O}_3\text{–}63.75\text{MoO}_3\text{–}15\text{B}_2\text{O}_3$ (RE: Sm, Gd, Dy) (mol%) were pre-

pared. Commercial powders of reagent grade Sm_2O_3 , Gd_2O_3 , Dy_2O_3 , MoO_3 , B_2O_3 were melted in a platinum crucible at 1000 °C for 40 min in an electric furnace. A small amount of CeO_2 (0.1 mol%) was added to reduce the dark brown color of $\text{RE}_2\text{O}_3\text{–MoO}_3\text{–B}_2\text{O}_3$ glasses. The melts were poured onto an iron plate and pressed to a thickness of 1–1.5 mm by another iron plate. Glass transition, T_g , and crystallization peak, T_p , temperatures were determined using differential thermal analysis (DTA) at a heating rate of 10 K/min. The quenched glasses were annealed at T_g to release internal stress and then polished mechanically to a mirror finish with CeO_2 powders.

The glasses were heat treated at T_p , and the crystalline phases present in the crystallized samples were identified by X-ray diffraction (XRD) analyses ($\text{CuK}\alpha$ radiation) at room temperature. Micro-Raman scattering spectra at room temperature for the precursor glasses and crystallized samples were measured with a laser microscope (Tokyo Instruments Co., Nanofinder) operated at Ar^+ (488 nm) laser. In our micro-Raman apparatus, the data below ~ 250 cm^{-1} cannot be measured due to the use of edge filter. Second harmonic (SH) intensities of crystallized powders at room temperature were evaluated using the powder method proposed by Kurtz and Perry [18]. A fundamental wave of a Q-switched Nd:YAG laser operating at a wavelength of $\lambda = 1064$ nm was used as the incident light. The SH intensity of α -quartz powders was used as a reference.

A cw Nd:YAG laser operating at 1064 nm was irradiated to the polished surface of the glasses with a mirror finish. The laser beam was focused on the surface of the glasses using an objective lens (magnification 20, numerical aperture NA = 0.4). By using a three-dimensional translation stage, focused positions of laser beam were moved at a constant speed. The laser powers were 0.6–0.95 W, and translation speeds of the sample stage were 1–16 $\mu\text{m/s}$. The surface morphology of crystal lines was examined from scanning confocal laser microscope (Olympus OLS3000) observations.

3. Results

3.1. Characterization of $\text{RE}_2\text{O}_3\text{–MoO}_3\text{–B}_2\text{O}_3$ glasses

The glass compositions examined in the present study are shown in Table 1. The glasses prepared are designated here as SMB for 21.25 $\text{Sm}_2\text{O}_3\text{–}63.75\text{MoO}_3\text{–}15\text{B}_2\text{O}_3$, GMB for 21.25 $\text{Gd}_2\text{O}_3\text{–}63.75\text{MoO}_3\text{–}15\text{B}_2\text{O}_3$, DMB for 21.25 $\text{Dy}_2\text{O}_3\text{–}63.75\text{MoO}_3\text{–}15\text{B}_2\text{O}_3$, SGMB for 10.625 $\text{Sm}_2\text{O}_3\text{–}10.625\text{Gd}_2\text{O}_3\text{–}63.75\text{MoO}_3\text{–}15\text{B}_2\text{O}_3$, and SDMB for 10.625 $\text{Sm}_2\text{O}_3\text{–}10.625\text{Dy}_2\text{O}_3\text{–}63.75\text{MoO}_3\text{–}15\text{B}_2\text{O}_3$. Furthermore, the glasses of 21.25 $\text{RE}_2\text{O}_3\text{–}63.75\text{MoO}_3\text{–}15\text{B}_2\text{O}_3$ (RE: Sm, Gd, Dy) are also designated here as RMB glasses. The DTA patterns for some bulk RMB glasses are shown in Fig. 1. The glasses show endothermic peaks due to the glass transition and exothermic peaks due to the crystallization. The values of T_g and T_p are summarized in Table 1. It is seen that the glass

Table 1

Glass compositions, values of glass transition T_g , and crystallization peak T_p temperatures in RE_2O_3 – MoO_3 – B_2O_3 glasses examined in the present study

Sample #	Glass (mol%)	T_g (°C) (± 2 °C)	T_p (°C) (± 2 °C)
SMB	21.25Sm ₂ O ₃ –63.75MoO ₃ –15B ₂ O ₃	526	572
GMB	21.25Gd ₂ O ₃ –63.75MoO ₃ –15B ₂ O ₃	536	585
DMB	21.25Dy ₂ O ₃ –63.75MoO ₃ –15B ₂ O ₃	536	589
SGMB	10.625Sm ₂ O ₃ –10.625Gd ₂ O ₃ –63.75MoO ₃ –15B ₂ O ₃	535	574
SDMB	10.625Sm ₂ O ₃ –10.625Dy ₂ O ₃ –63.75MoO ₃ –15B ₂ O ₃	530	579

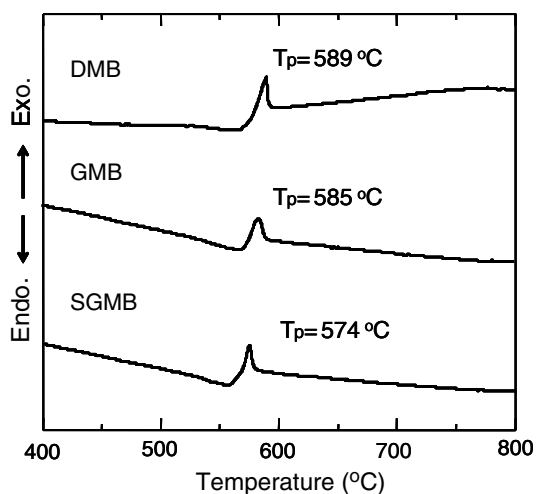


Fig. 1. DTA patterns for DMB, GMB, SGMB glasses. Heating rate was 10 K/min. DMB: 21.25Dy₂O₃–63.75MoO₃–15B₂O₃, GMB: 21.25Gd₂O₃–63.75MoO₃–15B₂O₃, SGMB: 10.625Sm₂O₃–10.625Gd₂O₃–63.75MoO₃–15B₂O₃. T_p is the crystallization peak temperature. The error in T_p is ± 2 °C.

transition and crystallization peak temperatures of RMB glasses are around 530 and 580 °C, respectively, being almost irrespective of RE_2O_3 species. The DTA patterns in Fig. 1 suggest the formation of one crystalline phase due to the crystallization.

The Raman scattering spectra at room temperature for RMB glasses are shown in Fig. 2. The peaks are broad,

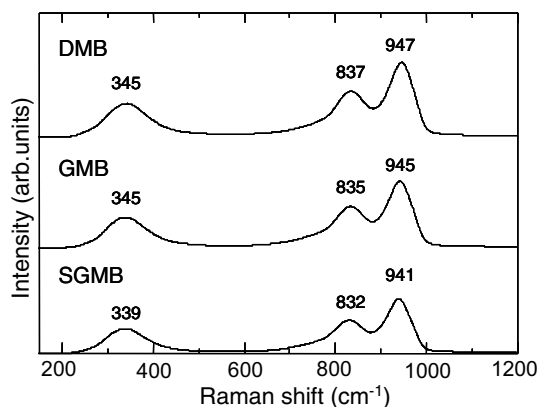


Fig. 2. Raman scattering spectra at room temperature for DMB, GMB, SGMB glasses. DMB: 21.25Dy₂O₃–63.75MoO₃–15B₂O₃, GMB: 21.25Gd₂O₃–63.75MoO₃–15B₂O₃, SGMB: 10.625Sm₂O₃–10.625Gd₂O₃–63.75MoO₃–15B₂O₃. The error in the peak positions is ± 2 cm⁻¹.

being typical for glass materials, and three kinds of peaks are observed at 339–345, 832–837, and 941–947 cm⁻¹. The Raman scattering spectra shown in Fig. 2 suggest that RMB glasses have similar glass structures, irrespective of RE_2O_3 species. It is known that the structural unit of MoO₄ tetrahedra in glasses gives the band at 840–850 cm⁻¹ in Raman scattering and infrared spectra [19,20]. Furthermore, isolated MoO₄ tetrahedra in molybdate crystals give the stretching vibration modes in the 750–1000 cm⁻¹ range and the bending modes in the 250–430 cm⁻¹ range [21]. On the other hand, MoO₆ octahedra in molybdate crystals show new bands in the 500–750 cm⁻¹ range [20]. The broad peaks shown in Fig. 2, therefore, suggest that MoO₄ tetrahedral units are formed in the RE_2O_3 – MoO_3 – B_2O_3 glasses containing of a large amount (63.75 mol%) of MoO₃ and act as network glass formers. Rare-earth oxides give Raman bands in the relatively low-frequency region below 400 cm⁻¹ [22], and it is considered that the band at ~ 345 cm⁻¹ would contain some contribution of the vibrations of REO_n polyhedra in the glasses.

3.2. Formation of β' - $RE_2(MoO_4)_3$ ferroelectrics by crystallization

The XRD patterns for the crystallized RMB samples obtained by heat treatment at T_p for 3 h are shown in Fig. 3. The peaks are assigned to β' - $RE_2(MoO_4)_3$ crystals, i.e., β' -Dy₂(MoO₄)₃, β' -Gd₂(MoO₄)₃, and β' -SmGd(MoO₄)₃ (JCPDS: No. 45-1216, No.20-408, No. 24-1000 and Ref. [10]). The phase diagram and structure of rare-earth molybdates, $RE_2(MoO_4)_3$, where RE = Pr, Nd, Sm, Eu, Gd, Tb, Dy, have been studied extensively [23–26]. The thermodynamically stable phase in the temperatures below 800–990 °C is the α phase with a monoclinic structure ($C2/c$). In the temperature range of 1000 < T < 1200 °C, the β phase with a tetragonal structure ($P4_21m$) is stable. The β phase (paraelectric) transforms to the β' phase (ferroelectric) with an orthorhombic structure ($Pba2$) below the Curie temperature [26].

Very recently, the Raman scattering spectra for the α -Sm₂(MoO₄)₃ and β' -Sm₂(MoO₄)₃ phases have been reported by Abe et al. [10]. The spectra reported are shown in Fig. 4, indicating that they change largely depending on the crystalline form. These data are useful for the discrimination between α - $RE_2(MoO_4)_3$ and β' - $RE_2(MoO_4)_3$

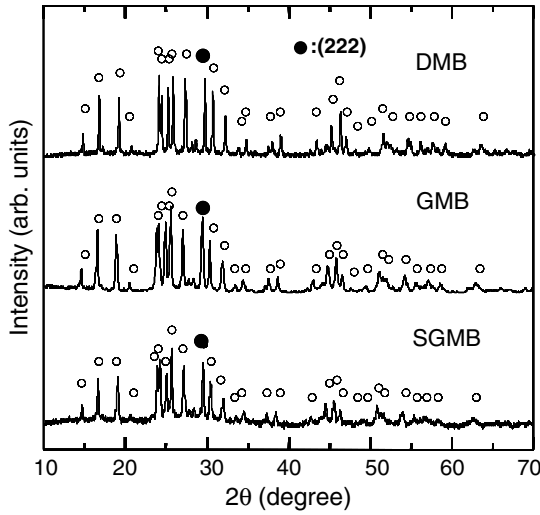


Fig. 3. XRD patterns at room temperature for the crystallized (at T_p for 3 h) samples of DMB, GMB, and SGMB glasses. The crystalline phase (open circle) is β' - $\text{RE}_2(\text{MoO}_4)_3$. DMB: $21.25\text{Dy}_2\text{O}_3-63.75\text{MoO}_3-15\text{B}_2\text{O}_3$, GMB: $21.25\text{Gd}_2\text{O}_3-63.75\text{MoO}_3-15\text{B}_2\text{O}_3$, SGMB: $10.625\text{Sm}_2\text{O}_3-10.625\text{Gd}_2\text{O}_3-63.75\text{MoO}_3-15\text{B}_2\text{O}_3$. The marked peak (●) corresponds to the (222) plane of β' - $\text{RE}_2(\text{MoO}_4)_3$ crystals.

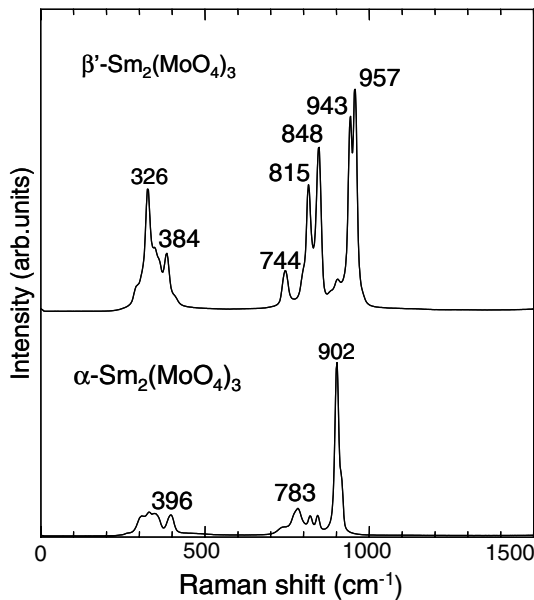


Fig. 4. Raman scattering spectra at room temperature for α - $\text{RE}_2(\text{MoO}_4)_3$ and β' - $\text{RE}_2(\text{MoO}_4)_3$ crystals prepared by solid state reaction. The data are taken from Ref. [10]. The error in the peak positions is $\pm 1 \text{ cm}^{-1}$.

phases present in the crystallized samples of $21.25\text{RE}_2\text{O}_3-63.75\text{MoO}_3-15\text{B}_2\text{O}_3$ glasses. The Raman scattering spectra for the crystallized samples obtained by heat treatment at T_p for 3 h are shown in Fig. 5. Comparing with the data shown in Figs. 4 and 5, it is clear that the Raman scattering spectra also indicate the formation of β' - $\text{RE}_2(\text{MoO}_4)_3$ crystals in these crystallized glasses. In the glasses examined in this study, the content of B_2O_3 is small, i.e., 15 mol%. Furthermore, as seen in Figs. 4 and 5, the crystallized glasses

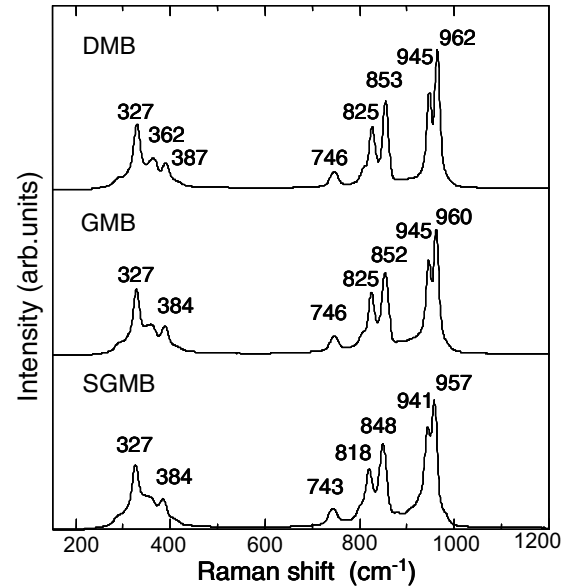


Fig. 5. Raman scattering spectra at room temperature for the crystallized (at T_p for 3 h) samples of DMB, GMB, and SGMB glasses. DMB: $21.25\text{Dy}_2\text{O}_3-63.75\text{MoO}_3-15\text{B}_2\text{O}_3$, GMB: $21.25\text{Gd}_2\text{O}_3-63.75\text{MoO}_3-15\text{B}_2\text{O}_3$, SGMB: $10.625\text{Sm}_2\text{O}_3-10.625\text{Gd}_2\text{O}_3-63.75\text{MoO}_3-15\text{B}_2\text{O}_3$. The error in the peak positions is $\pm 1 \text{ cm}^{-1}$.

show almost the same Raman scattering spectra as those for β' - $\text{RE}_2(\text{MoO}_4)_3$ ferroelectrics which were prepared by a solid state reaction. These results suggest that the contribution of BO_n units on the Raman scattering spectra shown in Fig. 5 might be extremely small. Indeed, we could not detect any clear peaks at $1000-1500 \text{ cm}^{-1}$, which are typical bands for pyroborate or orthoborate groups [27,28].

In the structure of the acentric orthorhombic β' - $\text{RE}_2(\text{MoO}_4)_3$ phase, REO_7 polyhedra (monocapped trigonal prisms) and MoO_4 tetrahedra are present and they are linked together via common corners [29]. It is, therefore, concluded that the Raman bands observed at ~ 327

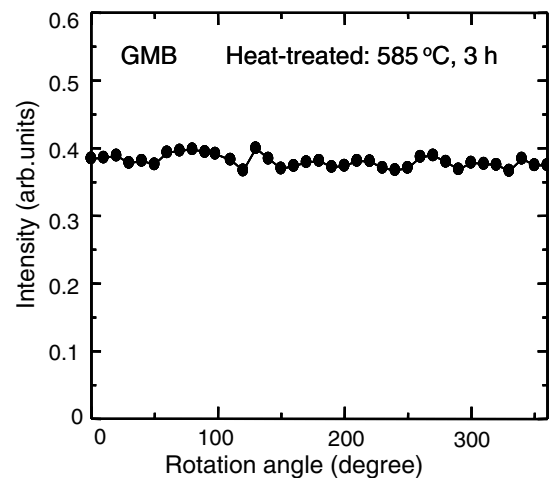


Fig. 6. Second harmonic intensities obtained by using Kurtz powder method for crystallized (at 585°C for 3 h) powder samples of GMB glass. GMB: $21.25\text{Gd}_2\text{O}_3-63.75\text{MoO}_3-15\text{B}_2\text{O}_3$.

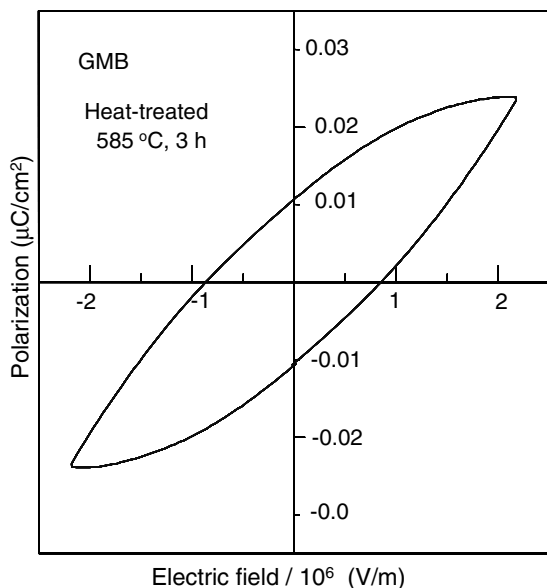


Fig. 7. Polarization (P)–electric field (E) hysteresis loop measured at 1 kHz for the crystallized (at 585 °C for 3 h) glass of GMB glass. GMB: 21.25Gd₂O₃–63.75MoO₃–15B₂O₃.

and $\sim 385\text{ cm}^{-1}$ in Fig. 6 correspond to the bending modes in MoO₄ tetrahedra in β' -RE₂(MoO₄)₃ crystals and those observed at ~ 820 , ~ 850 , ~ 945 , and $\sim 960\text{ cm}^{-1}$ are assigned to the stretching vibration modes in MoO₄ tetrahedra in β' -RE₂(MoO₄)₃ crystals [21].

The SH intensity for the crystallized RMB sample obtained by heat treatment at T_p for 3 h is shown in Fig. 6. In this experiment, the powdered samples (shaped to a disk plate) were rotated against incident measuring YAG laser to minimize the data scattering of SH intensity due to the inhomogeneous packing of powders. The result shown in Fig. 6 indicates that the crystals formed by crystallization are non-linear optical crystals. Kim et al. [30] examined the characteristics of the second harmonic generation (SHG) in Gd₂(MoO₄)₃ crystals grown by the Czochralski method and reported the value of $d_{\text{eff}} = 1.2 \pm 0.2\text{ pm/V}$ as the effective second order non-linear coefficient. Bonneville and Auzel [12] proposed that the major part of non-linear optical properties in β' -RE₂(MoO₄)₃ crystals is due to the orientation of MoO₄ tetrahedra and the Mo–O bond hyperpolarizability. On the other hand, Xue and Zhang [15] proposed that the major part of non-linear optical properties in β' -RE₂(MoO₄)₃ crystals is from the REO₇ groups. The interpretation of the origin of the anisotropic polarizability in β' -RE₂(MoO₄)₃ crystals is, therefore, still open to discussion. It should be pointed out that both MoO₃ and RE₂O₃ oxides show large electronic polarizabilities [31].

The polarization (P) for the crystallized RMB glass obtained by heat treatment at T_p for 3 h is shown in Fig. 7 as a function of electric field (E). The hysteresis is clearly observed in the P – E relation, indicating that the crystals formed by crystallization are ferroelectrics. The results (Figs. 3 and 5–7) obtained in the present study dem-

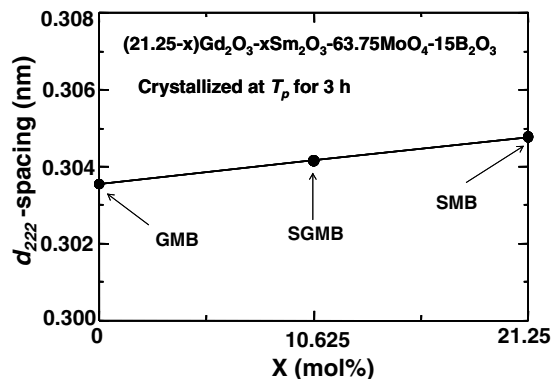


Fig. 8. Values of the d_{222} -spacing of β' -RE₂(MoO₄)₃ crystals formed in the crystallized (at T_p for 3 h) samples in (21.25 – x)Gd₂O₃– x Sm₂O₃–63.75MoO₃–15B₂O₃ glasses.

onstrate that the crystals formed in the crystallization of RE₂O₃–MoO₃–B₂O₃ glasses are ferroelectric and non-linear optical β' -RE₂(MoO₄)₃.

The values of the d_{222} -spacing for β' -RE₂(MoO₄)₃ crystals formed by heat treatment at T_p for 3 h in (21.25 – x)Gd₂O₃– x Sm₂O₃–63.75MoO₃–15B₂O₃ glasses ($x = 0, 10.625, 21.25$) are shown in Fig. 8, where these values were obtained by XRD analyses. It is seen that the d_{222} -spacing varies linearly with the Sm₂O₃/Gd₂O₃ ratio, indicating that the so-called Vegard' rule is hold. In other words, it is considered that β' -Gd_{2– x} Sm _{x} (MoO₄)₃ crystals are formed by crystallization and the ratio of rare-earth species in the crystals is controlled by the composition of precursor glasses.

3.3. Laser-induced crystallization of β' -RE₂(MoO₄)₃ ferroelectrics

As stated above, it was clarified that non-linear optical/ferroelectric β' -RE₂(MoO₄)₃ crystals (RE: Sm, Gd, Dy) are formed in 21.25RE₂O₃–63.75MoO₃–15B₂O₃ glasses by conventional crystallization in an electric furnace. Toward to the purpose of the present study, cw Nd:YAG lasers with $\lambda = 1064\text{ nm}$ were irradiated to RMB glasses. That is, the samarium atom heat processing was applied to the glasses. In this technique, the content of Sm₂O₃ or Dy₂O₃ in glass is one of the key points, and usually the content of around 8 mol% is needed to induce crystallization [6–10]. In this study, we, therefore, irradiated Nd:YAG lasers to SGMB, i.e., 10.625Sm₂O₃–10.625Gd₂O₃–63.75MoO₃–15B₂O₃, and SDMB, i.e., 10.625Sm₂O₃–10.625Dy₂O₃–63.75MoO₃–15B₂O₃, glasses.

The polarization optical micrograph (top view) and scanning confocal laser micrograph for the SGMB sample obtained by YAG laser irradiation are shown in Fig. 9, where the laser power was $P = 0.9\text{ W}$, the moving speed of the sample was $S = 10\text{ }\mu\text{m/s}$, and the laser was focused on the surface of the sample. It is seen that structural changes are induced by YAG laser irradiation. The surface of the laser irradiated part is not smooth, but periodic bumps are observed. The width of the line is about

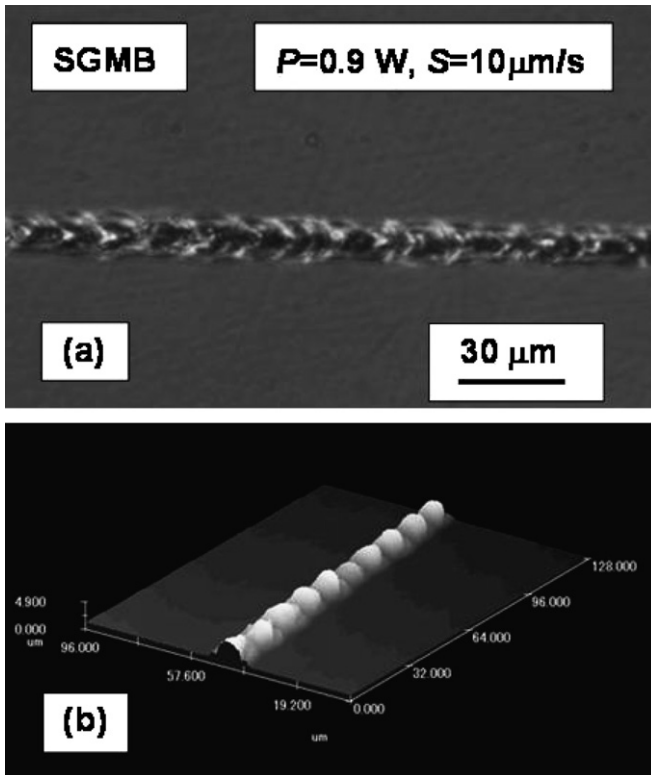


Fig. 9. Polarization optical (top views) (a) and laser confocal (b) micrographs for the SGMB sample obtained by cw Nd:YAG laser irradiation with a laser power of $P = 0.9$ W and sample moving speed of $S = 10$ $\mu\text{m/s}$. SGMB: $10.625\text{Sm}_2\text{O}_3\text{-}10.625\text{Gd}_2\text{O}_3\text{-}63.75\text{MoO}_3\text{-}15\text{B}_2\text{O}_3$.

13 μm , and the height of the bumps is about 4.8 μm . The micro-Raman scattering spectrum for the line is shown in Fig. 10, indicating that the line consists of β' - $\text{Gd}_{2-x}\text{Sm}_x(\text{MoO}_4)_3$ crystals. Since SGMB glass has the values of $T_g = 535$ and $T_p = 574$ $^\circ\text{C}$, it is considered that the temperature of the laser-irradiated region would be at least

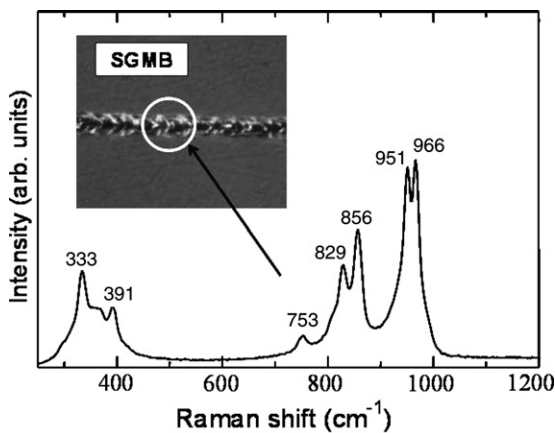


Fig. 10. Micro-Raman scattering spectrum at room temperature for the line written by cw Nd:YAG laser irradiation with a power of 0.9 W and a scanning speed of 10 $\mu\text{m/s}$ in SGMB glass. SGMB: $10.625\text{Sm}_2\text{O}_3\text{-}10.625\text{Gd}_2\text{O}_3\text{-}63.75\text{MoO}_3\text{-}15\text{B}_2\text{O}_3$. The error in the peak positions is ± 1 cm^{-1} .

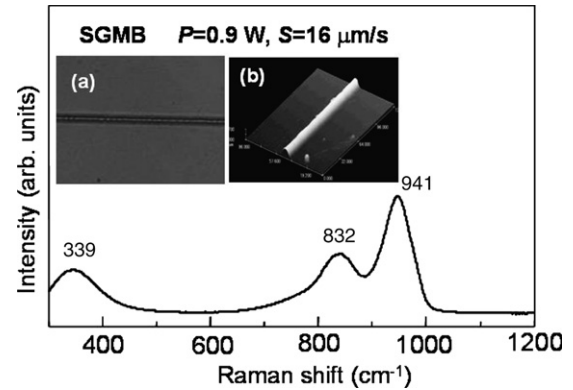


Fig. 11. Micro-Raman scattering spectrum at room temperature for the line written by cw Nd:YAG laser irradiation with a laser power of $P = 0.9$ W and sample moving speed of $S = 16$ $\mu\text{m/s}$. Polarization optical (top views) (a) and laser confocal (b) micrographs for the line are also included. SGMB: $10.625\text{Sm}_2\text{O}_3\text{-}10.625\text{Gd}_2\text{O}_3\text{-}63.75\text{MoO}_3\text{-}15\text{B}_2\text{O}_3$. The error in the peak positions is ± 2 cm^{-1} .

above 570 $^\circ\text{C}$. Furthermore, it is concluded that the scanning speed of $S = 10$ $\mu\text{m/s}$ would correspond to enough time to induce atomic rearrangements for crystallization.

The results on the polarization optical micrograph (top view), scanning confocal laser micrograph and the micro-Raman scattering spectrum for the line written by YAG laser irradiation with $P = 0.9$ W and $S = 16$ $\mu\text{m/s}$ in SGMB glass are shown in Fig. 11. In this condition, as can be seen in Fig. 11, the line does not consist of crystals but is still amorphous. It is considered that the fast scanning speed of 16 $\mu\text{m/s}$ means fast heating and cooling speeds of the laser-irradiated region, giving not enough time for atomic rearrangements for crystallization. It should be pointed out that the surface of this line is smooth. The width and height of the line is about 8 and 3.6 μm , respectively.

The polarization optical micrograph (top view) and scanning confocal laser micrograph for the SGMB sample obtained by YAG laser irradiation with $P = 0.73$ W and $S = 1$ $\mu\text{m/s}$ are shown in Fig. 12. In this condition, the structural change (width: ~ 10 μm , height: ~ 3.5 μm) with smooth surfaces is induced. The micro-Raman scattering spectrum for the line with the smooth surface is shown in Fig. 13. It is concluded that the line consists of both α - $\text{Gd}_{2-x}\text{Sm}_x(\text{MoO}_4)_3$ and β' - $\text{Gd}_{2-x}\text{Sm}_x(\text{MoO}_4)_3$ crystals.

The polarization optical micrograph (top view) and scanning confocal laser micrograph for the SDMB sample obtained by YAG laser irradiation with $P = 0.6$ W and $S = 10$ $\mu\text{m/s}$ are shown in Fig. 14. A structural change (width: ~ 16 μm , height: ~ 4.5 μm) with bumps similar to the case of SGMB glass (Fig. 8) is observed. From the micro-Raman scattering spectrum, it was confirmed that the line consists of β' - $\text{Dy}_{2-x}\text{Sm}_x(\text{MoO}_4)_3$ crystals. In the scanning speed of $S = 15$ $\mu\text{m/s}$, the line with the glassy state and a smooth surface was obtained, being similar to the case of SGMB glass (Fig. 10). We tried to write homogeneous crystal lines consisting of only β' - $\text{Dy}_{2-x}\text{Sm}_x(\text{MoO}_4)_3$

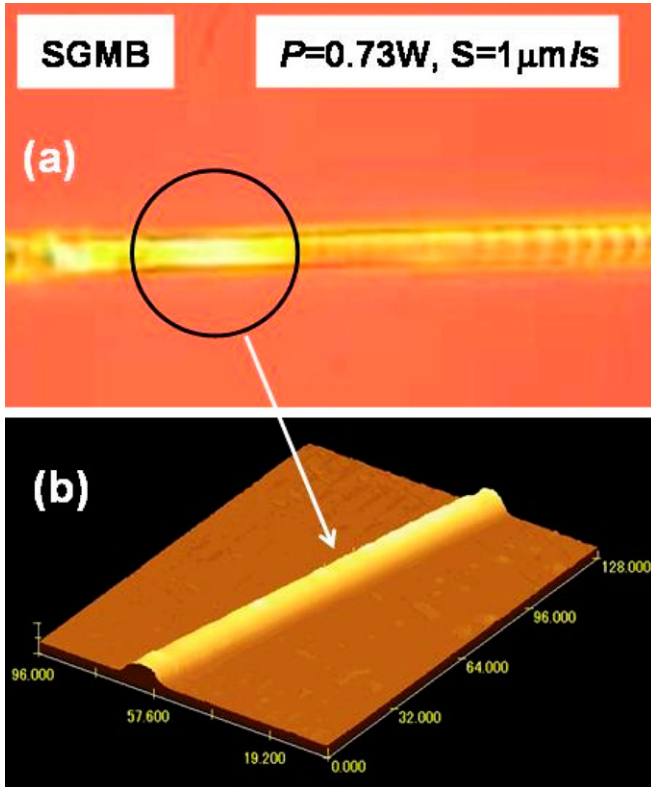


Fig. 12. Polarization optical (top views) (a) and laser confocal (b) micrographs for the SGMB sample obtained by cw Nd:YAG laser irradiation with a laser power of $P = 0.73$ W and sample moving speed of $S = 1$ $\mu\text{m/s}$. SGMB: $10.625\text{Sm}_2\text{O}_3\text{--}10.625\text{Gd}_2\text{O}_3\text{--}63.75\text{MoO}_3\text{--}15\text{B}_2\text{O}_3$.

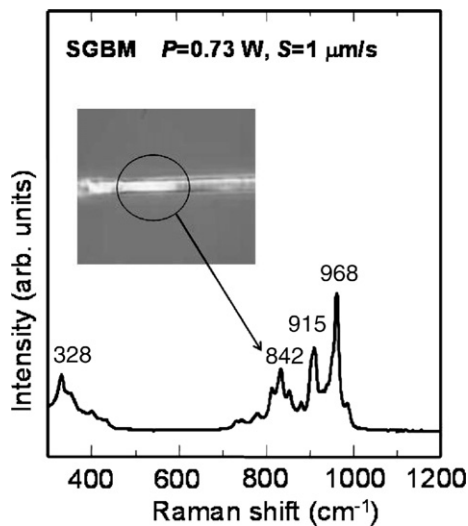


Fig. 13. Micro-Raman scattering spectrum at room temperature for the line written by YAG laser irradiation with a power of $P = 0.73$ W and a scanning speed of $S = 1$ $\mu\text{m/s}$ in SGMB glass. SGMB: $10.625\text{Sm}_2\text{O}_3\text{--}10.625\text{Gd}_2\text{O}_3\text{--}63.75\text{MoO}_3\text{--}15\text{B}_2\text{O}_3$. The error in the peak positions is ± 1 cm^{-1} .

crystals in various laser irradiation conditions, but at this moment such lines have not been obtained.

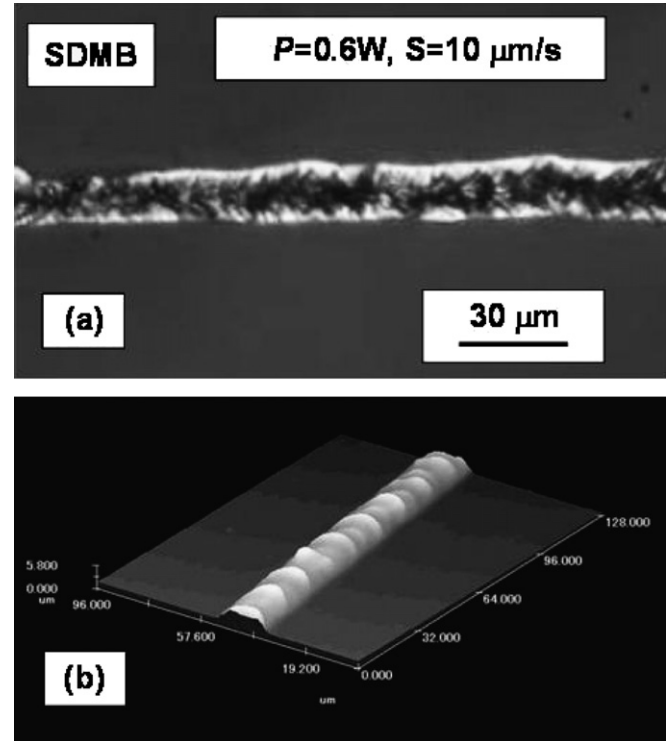


Fig. 14. Polarization optical (top views) (a) and laser confocal (b) micrographs for the SDMB sample obtained by cw Nd:YAG laser irradiation with a laser power of $P = 0.6$ W and sample moving speed of $S = 10$ $\mu\text{m/s}$. SDMB: $10.625\text{Sm}_2\text{O}_3\text{--}10.625\text{Dy}_2\text{O}_3\text{--}63.75\text{MoO}_3\text{--}15\text{B}_2\text{O}_3$.

4. Discussion

As indicated in the present study, the initial crystalline phase formed by the crystallization of $21.25\text{RE}_2\text{O}_3\text{--}63.75\text{MoO}_3\text{--}15\text{B}_2\text{O}_3$ glasses is not paraelectric $\alpha\text{-RE}_2(\text{MoO}_4)_3$ crystals, but ferroelectric $\beta'\text{-RE}_2(\text{MoO}_4)_3$ crystals. The glasses of $21.25\text{RE}_2\text{O}_3\text{--}63.75\text{MoO}_3\text{--}15\text{B}_2\text{O}_3$ have the values of $T_g \sim 530$ $^\circ\text{C}$ and $T_p \sim 580$ $^\circ\text{C}$. On the other hand, it is known that the thermodynamically stable phase in the temperatures below $800\text{--}990$ $^\circ\text{C}$ for $\text{RE}_2(\text{MoO}_4)_3$ crystals is the $\alpha\text{-RE}_2(\text{MoO}_4)_3$ phase [23–26]. The crystallization temperature of the glasses corresponds, therefore, to the formation region of the $\alpha\text{-RE}_2(\text{MoO}_4)_3$ phase. As seen in Figs. 2, 4, and 5, the Raman scattering spectra suggest that the structure of the glasses might be close to the structure of the $\beta'\text{-RE}_2(\text{MoO}_4)_3$ phase, but not to the $\alpha\text{-RE}_2(\text{MoO}_4)_3$ phase. This would be one of the reasons for the initial formation of $\beta'\text{-RE}_2(\text{MoO}_4)_3$ crystals in the glasses.

Irrespective of the heat treatment methods, i.e., conventional heat treatment in an electric furnace and laser-induced heating, basically $\beta'\text{-RE}_2(\text{MoO}_4)_3$ crystals are formed initially in the crystallization of $21.25\text{RE}_2\text{O}_3\text{--}63.75\text{MoO}_3\text{--}15\text{B}_2\text{O}_3$ glasses. In the crystallized glasses obtained by heat treatment at T_p for 3 h in an electric furnace, only $\beta'\text{-RE}_2(\text{MoO}_4)_3$ crystals are present, indicating no trace of $\alpha\text{-RE}_2(\text{MoO}_4)_3$ crystals (Figs. 3 and 5). Here, it should be pointed out that the heat treatment time is

3 h, relatively long. On the other hand, as seen in Figs. 12 and 13, the crystal line written by Nd:YAG laser irradiation with a power of $P = 0.73$ W and a laser scanning speed of $S = 1$ $\mu\text{m/s}$ consists of both $\alpha\text{-RE}_2(\text{MoO}_4)_3$ and $\beta'\text{-RE}_2(\text{MoO}_4)_3$ crystals. In this case ($S = 1$ $\mu\text{m/s}$), it would be reasonable to conclude that during the irradiation and scanning of Nd:YAG laser firstly $\beta'\text{-RE}_2(\text{MoO}_4)_3$ crystals are crystallized and then the transformation of some amounts of $\beta'\text{-RE}_2(\text{MoO}_4)_3$ crystals to $\alpha\text{-RE}_2(\text{MoO}_4)_3$ crystals occurs. According to Nassau et al. [24], the transformation from the α phase to the β phase occurs easily (fast), but the phase transition from the β phase to the α phase is slow kinetically. As seen in Fig. 9, the crystal line written by Nd:YAG laser irradiation with $P = 0.9$ W and $S = 10$ $\mu\text{m/s}$ consists of only $\beta'\text{-RE}_2(\text{MoO}_4)_3$ crystals, indicating no transformation to $\alpha\text{-RE}_2(\text{MoO}_4)_3$ crystals. It is considered that the scanning speed of 10 $\mu\text{m/s}$ does not give enough time for the transformation between these two phases. At this moment, the temperature of the YAG laser irradiated region in the glasses has not been determined. However, considering the results that the heat treatments for the long periods of 3 h at the crystallization temperatures in the glasses (Figs. 3 and 5) do not induce the transformation of $\beta'\text{-RE}_2(\text{MoO}_4)_3$ to $\alpha\text{-RE}_2(\text{MoO}_4)_3$ crystals, the temperature of the YAG laser irradiated region might be much higher than crystallization temperatures.

As seen in Figs. 9–14, the morphology of the crystal lines written by Nd:YAG laser irradiation varies largely with laser irradiation and scanning conditions. One of the main purposes in this study is to write homogeneous $\beta'\text{-RE}_2(\text{MoO}_4)_3$ single crystal lines at the surface of glasses. Although we tried to write $\beta'\text{-RE}_2(\text{MoO}_4)_3$ crystal lines in $21.25\text{RE}_2\text{O}_3\text{-}63.75\text{MoO}_3\text{-}15\text{B}_2\text{O}_3$ glasses with various Nd:YAG laser irradiation conditions, such target crystal lines have not been fabricated at this moment. Since the crystal growth rate in glasses depends strongly on glass composition, it would be of interest to write crystal lines in the modified glasses such as $20\text{RE}_2\text{O}_3\text{-}65\text{MoO}_3\text{-}5\text{BaO}$ (or $5\text{Na}_2\text{O}$)– $10\text{B}_2\text{O}_3$, and such a study is now in progress.

As seen in Fig. 12, another feature in the surface morphology of the crystal lines is that the surface swells about 3.5 μm from the glass surface. Prior to crystallization during YAG laser irradiation, the solid-state glass melts to the super-cooled liquid state. This means that a volume expansion to the free surface occurs, consequently giving a swell of the crystallized region [10]. For practical applications of ferroelectric $\beta'\text{-RE}_2(\text{MoO}_4)_3$ crystal lines such as tunable optical switching, we need to apply electric field in order to induce phase shift in the light transmitting crystal lines. A schematic illustration for such a model device is shown in Fig. 15. It is considered that a swell in the crystal lines is of great advantage to the fabrication of electrodes.

A key point in the samarium (rare-earth) atom heat processing is a combination of rare-earth ions and cw Nd:YAG laser with $\lambda = 1064$ nm, and it is, of course, prerequisite to prepare glasses with some amounts (\sim more than 8 mol%) of Sm_2O_3 (or Dy_2O_3). Considering the con-

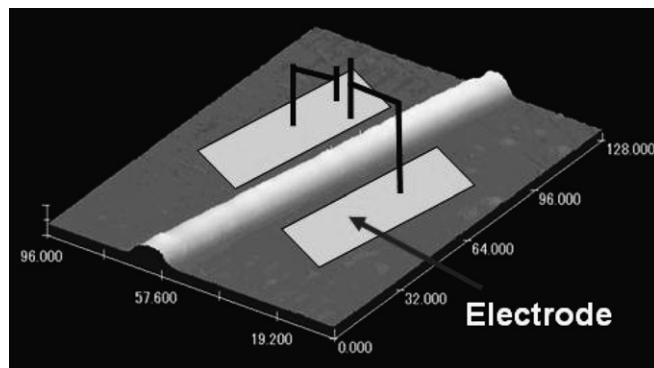


Fig. 15. A schematic illustration for a model device such as optical switching using a crystal line written by Nd:YAG laser irradiation.

cept of the samarium atom heat processing, other combinations would be possible for laser-induced crystallization in glass. Indeed, Gupta et al. [32] found that the irradiation of cw Ti-Sapphire laser with $\lambda = 800$ nm to $\text{Nd}_{0.2}\text{La}_{0.8}\text{BGeO}_5$ glass induces the formation of micron-size crystals. In this case, the 800 nm radiation is absorbed by Nd^{3+} ions. Since the heat dissipation from the laser-irradiated region to the surrounding glass medium occurs rapidly, it is necessary to irradiate laser continuously to keep high temperatures (greater than crystallization temperature) and thus to use continuous-wave type lasers for laser-induced crystallization in glass. Even in the RMB glasses prepared in this study, no crystallization was induced by using a nanopulse Nd:YAG laser with $\lambda = 1064$ nm.

5. Conclusions

The glasses with the compositions of $21.25\text{RE}_2\text{O}_3\text{-}63.75\text{MoO}_3\text{-}15\text{B}_2\text{O}_3$ (RE: Sm, Gd, Dy) were prepared and the formation of $\beta'\text{-RE}_2(\text{MoO}_4)_3$ ferroelectrics was confirmed in the crystallized glasses obtained through a conventional crystallization in an electric furnace. Cw Nd:YAG laser with $\lambda = 1064$ nm (laser power: $P = 0.6\text{-}0.9$ W, laser scanning speed: $S = 1\text{-}25$ $\mu\text{m/s}$) was irradiated to $10.625\text{Sm}_2\text{O}_3\text{-}10.625\text{Gd}_2\text{O}_3$ (or Dy_2O_3)– $63.75\text{MoO}_3\text{-}15\text{B}_2\text{O}_3$ glasses, and the structural modification was induced on the glass surface. In both glasses, crystal lines consisting of $\beta'\text{-Gd}_{2-x}\text{Sm}_x(\text{MoO}_4)_3$ and $\beta'\text{-Dy}_{2-x}\text{Sm}_x(\text{MoO}_4)_3$ crystals were patterned successfully at the glass surface. In particular, at the condition of $P = 0.73$ W and $S = 1$ $\mu\text{m/s}$, it was found that crystal lines consist of the mixture of paraelectric $\alpha\text{-Gd}_{2-x}\text{Sm}_x(\text{MoO}_4)_3$ and ferroelectric $\beta'\text{-Gd}_{2-x}\text{Sm}_x(\text{MoO}_4)_3$ crystals. It was also found that the surface morphology changes largely depending on laser irradiation conditions. Homogeneous crystal lines with $\beta'\text{-RE}_2(\text{MoO}_4)_3$ ferroelectrics have not been written in this study, and further research would be needed.

Acknowledgments

This work was supported from Ministry of Internal Affairs and Communications Strategic Information and

Communications R&D Promotion Programs (SCOPE), Grant-in-Aid for Scientific Research from the Ministry of Education, Science, Sports, Culture and Technology, Japan, and by the 21st Century Center of Excellence (COE) Program in Nagaoka University of Technology.

References

- [1] G.H. Beall, L.R. Pinckney, *J. Am. Ceram. Soc.* 82 (1995) 5.
- [2] D. Du, X. Liu, G. Korn, J. Squier, G. Mourou, *Appl. Phys. Lett.* 64 (1994) 3071.
- [3] K.M. Davis, K. Miura, N. Sugimoto, K. Hirao, *Opt. Lett.* 21 (1996) 1729.
- [4] C.B. Schaffer, A.O. Jamison, E. Mazur, *Appl. Phys. Lett.* 84 (2004) 1441.
- [5] H. Ebendorff-Heidepriem, *Opt. Mater.* 25 (2004) 109.
- [6] R. Sato, Y. Benino, T. Fujiwara, T. Komatsu, *J. Non-Cryst. Solids* 289 (2001) 228.
- [7] T. Honma, Y. Benino, T. Fujiwara, T. Komatsu, R. Sato, *Appl. Phys. Lett.* 82 (2003) 892.
- [8] T. Honma, Y. Benino, T. Fujiwara, T. Komatsu, R. Sato, *Appl. Phys. Lett.* 83 (2003) 2796.
- [9] R. Ihara, T. Honma, Y. Benino, T. Fujiwara, R. Sato, T. Komatsu, *Solid State Commun.* 136 (2005) 273.
- [10] M. Abe, Y. Benino, T. Fujiwara, T. Komatsu, R. Sato, *J. Appl. Phys.* 97 (2005) 123516.
- [11] H.J. Borchardt, P.E. Bierstedt, *Appl. Phys. Lett.* 8 (1966) 50.
- [12] R. Bonneville, F.J. Auzel, *J. Chem. Phys.* 67 (1977) 4597.
- [13] A.A. Berezhnoi, *Opt. Spectrosc.* 77 (1994) 548.
- [14] H. Nishioka, W. Odajima, M. Tateno, K. Ueda, A.A. Kaminskii, A.V. Butashin, S.N. Bagayev, A.A. Pavlyuk, *Appl. Phys. Lett.* 70 (1997) 1366.
- [15] D. Xue, S. Zhang, *J. Phys. Chem. Solids* 59 (1998) 1337.
- [16] A.A. Kaminskii, *Phys. Stat. Sol. A* 149 (1995) K39.
- [17] A.A. Kaminskii, H.J. Eichler, D. Grebe, R. Macdonald, S.N. Bagaev, A.A. Pavlyuk, F.A. Kuznetsov, *Phys. Stat. Sol. A* 153 (1996) 1.
- [18] S.K. Kurtz, T.T. Perry, *J. Appl. Phys.* 39 (1968) 3798.
- [19] R. Iordanova, Y. Dimitriev, V. Dimitrov, D. Klissurski, *J. Non-Cryst. Solids* 167 (1994) 74.
- [20] A. Mogus-Milankovic, A. Santic, A. Gajovic, D.E. Day, *J. Non-Cryst. Solids* 325 (2003) 76.
- [21] M. Maczka, *J. Solid State Chem.* 129 (1977) 287.
- [22] T. Honma, Y. Benino, T. Fujiwara, T. Komatsu, R. Sato, V. Dimitrov, *J. Appl. Phys.* 91 (2002) 2942.
- [23] K. Nassau, H.J. Levinstein, G.M. Loiacono, *J. Phys. Chem. Solids* 26 (1965) 1805.
- [24] K. Nassau, J.W. Shiever, E.T. Keve, *J. Solid State Chem.* 3 (1971) 411.
- [25] W. Jeitschko, *Acta Crystallogr., Sect. B* 28 (1972) 60.
- [26] V. Dimitriev, V. Sinitsyn, R. Dilanian, D. Machon, A. Kuznetsov, E. Ponyatovsky, G. Lucazeau, H.P. Weber, *J. Phys. Chem. Solids* 64 (2003) 307.
- [27] B.N. Meera, J. Ramakrishna, *J. Non-Cryst. Solids* 159 (1993) 1.
- [28] H.R. Xia, P. Zhao, X.F. Cheng, W.L. Liu, S.J. Zhang, Z.X. Cheng, Z.H. Yang, *J. Appl. Phys.* 95 (2004) 5383.
- [29] A.A. Kaminskii, A.V. Butashin, H.J. Eichler, D. Grebe, R. Macdonald, K. Ueda, H. Nishiguchi, W. Odajima, M. Tateno, J. Song, M. Musha, S.N. Bagaev, A.A. Pavlyuk, *Opt. Mater.* 7 (1997) 59.
- [30] S.I. Kim, J. Kim, S.C. Kim, S.I. Yun, T.Y. Kwon, *Mater. Lett.* 25 (1995) 195.
- [31] V. Dimitrov, S. Sakka, *J. Appl. Phys.* 79 (1996) 1736.
- [32] P. Gupta, H. Jain, D.B. Williams, J. Toulouse, I. Veltchev, *Opt. Mater.*, in press.